Right coronary artery ligation in mice: A novel method to investigate right ventricular dysfunction and biventricular interaction.

Pierre SICARD[1], **Timothée JOUITTEAU**[1-2], **Thales ANDRADE-MARTINS**[1-3], **Abdallah MASSAD**[1], **Glaucy RODRIGUES de ARAUJO**[3], **Hélène DAVID**[1,2], **Lucile MIQUEROL**[4], **Pascal COLSON**[2], **Sylvain RICHARD**[1]

1- INSERM, CNRS, Université de Montpellier, PHYMEDEXP, Montpellier, France

2- Department of Anaesthesiology and Critical Care Medicine, Arnaud de Villeneuve Academic Hospital, F-34295 Montpellier, France

3- CiPharma, Escola de Farmácia, Universidade Federal de Ouro Preto, Minas Gerais, Brazil

4- Aix-Marseille University, CNRS, IBDM, 13288 Marseille, France

Running Title: Right coronary artery ligation in mice

Word count: 4843

**Corresponding author:*

Dr. Pierre SICARD,

INSERM, CNRS, Université de Montpellier, PHYMEDEXP

CHU Arnaud De Villeneuve Bât Crastes de Paulet

371 Avenue du Doyen Gaston Giraud

34295 Montpellier cedex

E-mail: pierre.sicard@inserm.fr; sicard123@yahoo.fr

Abstract

Right ventricular (RV) dysfunction can lead to complications following acute inferior myocardial infarction (MI). However, it is unclear how RV failure after MI contributes to left-sided dysfunction is unclear. The aim of this study was to investigate the consequences of right coronary artery (RCA) ligation in mice. RCA ligation was performed in C57BL/6JRj mice (n=38). The cardiac phenotypes were characterized using high-resolution echocardiography performed up to 4 weeks post-RCA ligation. Infarct size was measured using 2,3,5-triphenyltetrazolium chloride (TTC)-staining 24h post-RCA ligation and the extent of the fibrotic area was determined 4 weeks after MI. RV dysfunction was confirmed 24h post RCA ligation by a decrease in the tricuspid annular plane systolic excursion ($p<0.001$) and RV longitudinal strain analysis ($p<0.001$). Infarct size measured *ex-vivo* represented 45.1±9.1% of RV free wall. RCA permanent ligation increased RV/LV area ratio ($p<0.01$). Septum hypertrophy ($p<0.01$) was associated with diastolic septal flattening. During the 4 weeks post-RCA ligation, the LV ejection fraction was preserved, yet it was associated with impaired LV diastolic parameters (E/e', global strain rate during early diastole). Histological staining after 4 weeks confirmed the remodelling process with a thin and fibrotic RV. This study validates that RCA ligation in mice is feasible and induces right ventricular heart failure associated with development of LV diastolic dysfunction. Our model offers a new opportunity to study mechanisms and treatments of RV/LV dysfunction after MI.

NEW & NOTEWORTHY:

RV dysfunction frequently causes complications after acute inferior MI. How RV failure contributes to left-sided dysfunction is elusive because of the lack of models to study molecular mechanisms. Here, we created a new model of MI by tying permanently the RCA

in mice. This model offers a new opportunity to unravel mechanisms underlying RV/LV dysfunction and evaluate drug therapy.

Keywords:

Right ventricular infarction model, diastolic dysfunction, cardiomyocytes

Classifications:

Pathophysiology; Heart failure

Introduction

Long considered a simple pipe feeding the pulmonary arteries, the right ventricle (RV) is now acknowledged as a main actor of the heart. Despite an increasing interest for its role in pulmonary artery hypertension, injuries following RV infarction have been neglected. RV myocardial infarction (MI) is a specific event, which rarely occurs on its own. RV MI complicates 30 to 50% of inferior left ventricular (LV) infarction and is recognized in this situation as a major prognostic factor (13, 18, 28). RV infraction is associated with a higher incidence of conduction disturbance, ventricular arrhythmias, cardiogenic shock and short-term death (19). Despite the fact that the RV MI patient presents a better recovery than LV MI (1, 29), the mechanisms of RV dysfunction and remodelling remain unclear (32). Recent studies have shown that diastolic and systolic ventricular interactions are negatively influenced by the RV regional inhomogeneity and prolongation of contraction. This right-to-left ventricular interaction, integrated into the concept of biventricular interdependence (3), is notably linked to septal wall sharing, RV architecture participation in LV work and reduction of LV preload by RV inefficiency (15). In addition, RV ischemia could directly impair left ventricular contractility (5). However, the mechanisms that determine whether RV failure contributes to left-sided dysfunction are not well defined. Tantalizingly, small animal models of RV infarction induced by RCA ligation are currently unavailable, as the most common rodent model used by researchers to address MI remodelling is the permanent occlusion of the left descending coronary artery. In contrast to large animal models, (14, 21, 26) a mouse model of RV infarction should be more effective to study molecular mechanisms of RV dysfunction and remodeling after MI. The aim of this study was to develop and validate a mouse model of RV infarction through right coronary artery (RCA) ligation and investigate its consequences on LV function.

Methods

In vivo right ventricular ischemia mice model

Seventy-seven male C57BL/6JRj mice were anesthetized by 2% isofluorane inhalation with analgesia (buprenorphine 0.1 mg/kg s.c), and ventilated by orotracheal intubation (minivent, Harvard apparatus, USA). A specific procedure was designed in order to minimize the size of the thoracotomy and to limit

bleeding during RCA ligation, especially during the delicate maneuver of revealing the RCA by maintaining the right atrium. A small incision (2 cm) was made through the skin over the right chest (Figure 1 A). After dissection, cauterization and retraction of the pectoral major and minor muscle, the fourth intercostal space was exposed (Figure 2B). An incision was made at the fourth intercostal space with a cauterization tool to open the pleural membrane (Figure 1C). The right side of the heart was exposed and a sterile compress was used to maintain the right atrium (Figure 1D-E). The RCA was sutured, and ligated at a site ≈3-5 mm from its origin using a 9-0 nylon suture (Figure1 F-H) (n=43). Ischemia was verified by the sudden regional paleness of the myocardium and ST elevation (Figure 1 I). The thoracotomy site was closed while increasing positive end expiratory pressure. Only RCA ligation was omitted in the sham procedure (n=34). A movie of this new method of MI available in the Online Data Supplement.

The Animal Care and Use Committees of the University of Montpellier (CEEA-LR-1435-13129) approved all animal experiments. Mice were housed in a pathogen-free facility and handled in accordance with the principles and procedures outlined in the ARRIVE guidelines (20) and in the *American Journal of Physiology* guidelines for experimental models of myocardial ischemia and infarction (23). In order to minimize the number of animals used per experiment in our study, we used only male mice. Moreover, this investigation conformed to the guidelines for ethical care of experimental animals of the European Union (2010/63/EU).

Echocardiography and speckle tracking analysis

High-resolution echocardiography (VisualSonics/Fujifilm, Canada with a MS550D ultrasound probe 40 MHz) was performed under anaesthesia by 2% isofluorane inhalation at 37°C, ECG and respiratory rate were monitored.

The mitral valve leaflet was visualized and mitral flow (Mitral valve (MV) flow and MV tissular Doppler) was assessed at long axis b-mode view by placing the transducer on the left lateral chest wall were recorded using pulse wave Doppler. Wall thicknesses, end-systolic and end-diastolic LV dimensions were measured according the *American Physiological Society* guidelines as applied to mice (24). LV wall thickness was measured at the level of intraventricular septum and posterior wall.

LV volume was calculated from Simpson's method of disks and ejection fraction determined from the formula (LV end-diastolic-end-systolic volume)/(LV end-diastolic volume). Longitudinal strain analysis was performed under long axis view, whereas circumferential strain analysis was performed under short axis view.

A four-chamber view was used to characterize the RV function with the Tricuspid annular plane systolic excursion (TAPSE) measurement. Speckle tracking analysis was used to study global and regional RV strain modification. We specifically used left atrium area, Isovolumic Relaxation Time (IVRT), peak early filling (E wave) and late diastolic filling (A wave) ratio (E/A), early filling (E) to early diastolic mitral annular velocity (E') (E/E' ratio), E wave and end diastolic strain rate ratio (E/SRe) to determine diastolic function index (33, 35, 36). Offline image analyses were performed using dedicated VisualSonics Vevolab 3.1.0 software.

Infarct size

Triphenyltetrazolium chloride (TTC) staining was realized 24 hours post-MI. Five mice per group were euthanized with pentobarbital (300 mg/kg) and heparin (150 U) intraperitoneally and the heart was quickly excised, sliced into four 1.0-mm-thick sections perpendicular to the long axis of the heart. The sections were then incubated with 1% TTC at 37°C for 10 min and then scanned. The infarct area was measured using ImageJ software and myocardial infarct sizes were expressed as a percentage of the right ventricle area (n=7 /group).

Histology

Four weeks after permanent RCA ligation, hearts were dissected, fixed for four hours in 4% paraformaldehyde (vol/vol) in PBS, washed in sucrose gradient, then embedded in OCT and cryosectioned. Hearts were observed under a Zeiss Apotome microscope. Fibrotic area was determined with wheat germ agglutinin-Cy3 (WGA-Cy3 from Sigma-Aldrich) as described previously (7, 25). To measure interventricular wall septum thickness, three sections from each heart were analyzed with ImageJ software. For each section, six different measurements

were taken along the septum, and results were represented as average of heart wall thickness of IVS (n=7 /group).

Single-cell contractility

Four weeks after surgery, single RV, LV and septal myocytes were isolated by enzymatic digestion from sham and RCA ligation heart. Hearts were rapidly excised after euthanasia (cervical dislocation) and submitted to enzymatic action (liberase) using a Langendorff perfusion system in order to disperse single rod-shaped left ventricular (LV) myocytes (10, 25). Only cardiomyocytes with clear edges and quiescent were used within 1–4 h of isolation for experiments. Unloaded cell shortening was measured (Sarcomere length, SL; IonOptix system, Hilton, USA) during field stimulation (1-ms current pulses at 0.5 Hz, room temperature 22 °C ±2 °C, 1.8 mM external Ca^{2+}). Data were analyzed using Ionwizard Software.

Statistical analysis

Results are expressed as mean ± SEM. Kaplan-Meier survival curves plot of the Sham (n = 24) and RCA ligation mice (n=33), where the outcome is time until 4 weeks (Log-rank Mantel-Cox test). Experimental groups were compared using the Mann-Whitney test for independent samples. A value of $p<0.05$ was considered significant. Analyses were performed using the GraphPad Prism 6 software.

Results

Surgical procedure and survival analysis

A total of 57 mice were used in the MI survival study. The average procedure time was 30.4±1.5 min for sham and 31.2±2.1 minutes for RCA ligation. Surgical approach differed from classical LCA ligation firstly in the right thoracic access, and especially in the delicate maneuver of revealing the RCA by maintaining the right atrium as shown in Figure 1 D-E and supplemental video 1.

During the peri-surgical period (from the beginning of surgery to 6 hours after), three mice died (12.5%) in the sham group and five mice died (15.1%) in the RCA ligation group (Figure 1 J).

Causes of death were bleeding (6 mice) and pneumothorax (2 mice). After the peri-surgical period, no mice died in the sham group and 2 mice (7.7%) died in the RCA ligation group (Figure 1 K). The reason for those deaths was not identified, yet we assume that this can be attributed to either cardiac arrhythmia or sudden cardiac arrest because autopsy of these mice showed no blood in the thoracic cavity. The overall survival rates (excluding surgical-related death) were 100% in sham group and 74% if peri-surgical death was not included (p=0.133).

RCA permanent occlusion induced RV dysfunction

We used high-resolution ultrasound as a non-invasive method to measure RV function 24h hour, 1 week and 4 weeks after permanent RCA occlusion. As shown in Figure 2 A, the RCA ligation group exhibited severely impaired and akinetic RV motion compared to sham mice (RV global longitudinal strain (-12.7±0.8 *vs.* -8.8±0.9, $p<0.001$) especially in the mid base part of free RV wall (Figure 2 B, $p<0.003$) while the apex longitudinal strain was progressively restored 4 weeks post-MI. In addition, the TAPSE was decreased (Figure 2 C) during the follow up. RV and RA were clearly dilated 24h post-surgery and even more after 28 days post-MI (Figure 2 D-E, Figure 4 E). Heart rates were similar among all of the groups (503.4 ± 52.1 *vs.* 487.6 ± 12.9 bpm, p=0.367). Overall, we observed an acute and global deterioration of RV function parameters after ligation of its main artery. We investigated single cell shortening, measured as a variation of SL (Figure 2 F-J). At rest, SL was unchanged (Panel F). However, a decreased in cell peak shortening ($p<0.0001$) (Panel G) and late acceleration ($p<0.0001$) (Panel H) and deceleration ($p<0.0001$) (Panel I) were observed, reflecting impaired single cell contraction (Panel J). Consistent with the echocardiographic observations, histologic analysis with TTC staining confirmed systematic RV infarction in RCA-L group, which was absent in sham mice. Infarct size was homogeneous between RCA-L mice and represented less than 50% of the RV (Figure 2 K). We performed histological assessment of RV infarction at 4 weeks post-MI as shown in Figure 2 L. RCA-L group presented a thinner fibrotic RV free wall in nearly half of the RV (Figure 2 L-M). We did not identify major interstitial fibrosis in the septum or LV compared to Sham mice.

Segmental behaviour in the LV: hypertrophy and hyperkinesia of the septum

Between the left and the right ventricle, the septum appears as the keystone of bi-ventricular interaction (34). In our model, RV dysfunction and dilation caused leftward deviation of the interventricular septum (a D-shaped septum is shown in Figure 3 A) especially during diastole and respiratory phase (supplemental videos 2 and 4 for sham, compared to supplemental video 3 and 5 for RCA ligation mice). In addition, the septal wall was thickened by nearly 20% (Figure 2 N and Figure 3 B) and septal contractility, estimated by circumferential strain (Figure 3 C) and strain rate (Figure 3 D), was improved 4 weeks after RCA ligation compared to Sham mice. The peak of early diastolic strain rate was measured for septal segment (figure 3 E) and revealed a better septal relaxation index after RCA ligation compared to Sham mice ($p<0.05$). We next decided to isolate septal ventricular cardiomyocytes and study their contractility (Figure 3 F-J). Septal cardiomyocytes from RCA Ligation mice exhibited higher peak rate of cell shortening compared to Sham cardiomyocytes ($p<0.0004$) (Panel G, J). In addition, velocity of shortening was improved ($p<0.017$) (Panel I, J).

RCA ligation induced left ventricular diastolic dysfunction

It is well known that RV failure and septal D-shaped is associated with LV dysfunction (6). We assessed, through echocardiography, the LV systolic and diastolic functions. LV ejection fraction and global longitudinal strain (systolic function) were preserved (Figure 4 A,B) over time despite RCA ligation. However, cardiac output decreased 4 weeks after RCA ligation (Figure 4 C), and was associated with a reduction of Left Ventricular Internal Size (LVID) in both systole and diastole in the RCA ligation group (Figure 4 D). Heart rate (503.4 ± 52.1 *vs.* 487.6 ± 12.9 bpm, $p=0.367$), thickness of left anterior wall (LVAW) and Left Ventricular Posterior Wall (LVPW) were similar between both groups (LVAWd: 0.91 ± 0.02 mm Sham vs 0.96 ± 0.02 mm RCA lig, $p=0.115$; LVPWd: 0.82 ± 0.03 mm Sham vs. 0.87 ± 0.04 mm RCA lig; $p=0.07$).

Mice from the RCA Ligation group presented several characteristics for LV diastolic dysfunction, with an increased left and right atrium area (Figure 4 E), a prolonged IVRT (Figure 4 F), a reduction of E/A ratio (Figure 4G). The E/E' (Figure 4 H) and E/SRE ratios (Figure 4I) were both increased.

Contraction of LV cardiomyocytes from the RCA ligation group showed no major modification compared to that of cardiomyocytes isolated from Sham animals (Figure 4 J-N). Only a slight increase in the contraction time for maximal amplitude was evidenced between the two groups (Panel L and N).

Taken together, our results demonstrate that this model of MI achieved by RCA ligation in mice is feasible, inducing right ventricular dysfunction associated with septal adaptation and a flawed LV diastolic function.

Discussion

To our knowledge, this is the first description of a murine model of RCA ligation. The surgery provoked an important RV infarction without LV ischemic injuries. Mice presented RV systolic function breakdown and morphological alterations, with RV dilatation and inversion of RV/LV area ratio. In contrast to the LAD ligation procedure in mice (23, 25), the RCA is more difficult to access. The method to properly ligate properly the RCA is challenging because of the thickness of the RV wall and the proximity of the right atrium, which makes the surgical gesture critical. Despite necessary surgical training, the protocol is reliable with systematic infarction, reproductive, as well as safe with a low mortality. Mice can survive several weeks after ligation permitting longitudinal follow-up. RV infarction was associated with an echocardiographic pattern of RV failure. In our hands, achievement of RV infarct size (approximately 50% of the RV free wall) was consistent and comparable to *ex-vivo* model of global ischemia on isolated heart rats (2).

After 4 weeks follow-up, RCA ligation mice still displayed an impaired RV systolic function with reduced TAPSE and longitudinal strain, although these parameters were improved compared to their early assessment. This corroborates medical data concerning RV improvement after infarction (17). Within the RV, areas presented a distinct profile. Apex longitudinal strain recovered progressively while free wall longitudinal strain remained low. RV/LV area ratio was still increasing, but the dispersion of data evokes various remodelling profiles or status after infarction, or/and different infarction seriousness. Partial normalization of RV systolic parameters seen after 4 weeks follow-up corroborates observations about RV recovery following infarction in human and supports clinical

relevance of this model (17). Compared to LV infarction, the improvement of the RV function may be caused by lower afterload, better left to right collateral flow and systolo-diastolic perfusion. It is interesting to note that the RV is more resilient against ischemia than the LV. The right ventricle needs lower myocardial oxygen demand and a better oxygen supply and coronary perfusion throughout the cardiac cycle (30). The RV, unlike the LV, has an oxygen extraction reserve, which works as an additional defence mechanism against myocardial ischemia (8).

In our model, classical LV systolic parameters remained unchanged over time. This suggests there is no major ischemic remodelling process affecting LV systolic parameters. Our late segmental analysis reports a hyperkinetic and hypertrophic septum wall, contrary to the lateral wall. This could be part of the adaptive hypertrophic mechanism in reaction to RV failure. Diastolic dysfunction presents a complex pattern. First, there is a pattern of impaired relaxation, as described in models of diastolic dysfunction in mice, specifically those involving hypertrophy and pressure overload (35). Secondly, moderate increase of E/E' and E/SRE evokes an elevation of LV filling pressure, which is explained by two mechanisms: septal hypertrophy associated with fibrosis and dilatation of the RV within the restricted intra-pericardial space impairing LV filling. Acute and chronic RV dysfunction influence LV function because the two ventricles work in series but are anatomically arranged in parallel, sharing a common ventricular septum (11, 34). Under these conditions, during the end-diastolic phase, there is a leftward displacement of the interventricular septum producing distortion of the short-axis profile of the LV. It is worth to note that RV systolic dysfunction is present in 15% of human myocardial infarction (MI), mostly for patients with pluri-troncular coronary lesions. Moreover, RCA is the culprit coronary artery in one-third of MI (4). Interestingly, women have RV MI more frequently than men (27). Gender plays a major role in cardiovascular disease evolution, especially for HF with preserved ejection fraction that affects more women than men (9). This aspect warrants further investigation.

Overall, this study provides interesting and novel data about chronic remodelling after isolated RV infarction. There was a deficit of knowledge because isolated RV ischemia rarely occurs in human (12). We also unravelled development of LV diastolic dysfunction after RCA permanent ligation. Among the few studies in large animal models of chronic RV failure after RCA occlusion (5, 14, 16,

21, 22, 26, 31) only one reported that RV failure induces LV systolic dysfunction (5). We assumed that different perfusion networks between animals and fewer collateral perfusion are responsible for that differences. Large mammalian models (dogs, sheep, pigs) share many cardiovascular characteristics with human, but have a high cost of housing and maintenance. In comparison, mice are easy to handle and housing. In addition, murine models can be easily genetically modified (e.g. Knock out, Knock in mice) allowing for the study of remodelling molecular mechanisms during RV failure.

In conclusion, we developed a new model of selective RV infarction, which allows the investigation of RV adaptation during and after ischemia. This approach could provide valuable information for preclinical mechanistic studies and drug therapy evaluation.

Funding

This work was supported by grants from INSERM, CNRS, Université de Montpellier, a Bilateral Research Collaborative program CAPES-COFECUB between Brazil and France (n°768/13 to SR; PhD grant to TM, post-doctoral grant to GRdA) and by grant from the Fondation Leducq (RETP).

Acknowledgments

We gratefully thank Patrice BIDEAUX and the staff for animal housing (PhyMedExp). We thank *Imagerie du Petit Animal de Montpellier* (IPAM) for the access to high resolution ultrasound.

Conflict of interest

The authors have declared that no competing interests exist.

References

1. **Albulushi A, Giannopoulos A, Kafkas N, Dragasis S, Pavlides G, Chatzizisis YS**. Acute right ventricular myocardial infarction. *Expert Rev Cardiovasc Ther* 16: 1–10, 2018.
2. **Andersen A, Povlsen JA, Bøtker HE, Nielsen-Kudsk JE**. Ischemic preconditioning reduces right ventricular infarct size through opening of mitochondrial potassium channels. *Cardiology* 123: 177–180, 2012.
3. **Bernheim P**. De l'asystolie veineuse dans l'hypertrophie du coeur gauche par stenose concomitante du ventricule droit. . *Rev Med (Paris)* : 785–801, 1910.
4. **Bowers TR, O'Neill WW, Pica M, Goldstein JA**. Patterns of coronary compromise resulting in acute right ventricular ischemic dysfunction. *Circulation* 106: 1104–1109, 2002.

5. **Brookes C, Ravn H, White P, Moeldrup U, Oldershaw P, Redington A**. Acute right ventricular dilatation in response to ischemia significantly impairs left ventricular systolic performance. *Circulation* 100: 761–767, 1999.
6. **Cativo Calderon EH, Mene-Afejuku TO, Valvani R, Cativo DP, Tripathi D, Reyes HA, Mushiyev S**. D-Shaped Left Ventricle, Anatomic, and Physiologic Implications. *Case reports in cardiology* 2017: 4309165, 2017.
7. **Choquet C, Nguyen THM, Sicard P, Buttigieg E, Tran TT, Kober F, Varlet I, Sturny R, Costa MW, Harvey RP, Nguyen C, Rihet P, Richard S, Bernard M, Kelly RG, Lalevée N, Miquerol L**. Deletion of Nkx2-5 in trabecular myocardium reveals the developmental origins of pathological heterogeneity associated with ventricular non-compaction cardiomyopathy. *PLoS Genet* 14: e1007502, 2018.
8. **Crystal GJ, Pagel PS**. Right ventricular perfusion: physiology and clinical implications. *Anesthesiology* 128: 202–218, 2018.
9. **Duca F, Zotter-Tufaro C, Kammerlander AA, Aschauer S, Binder C, Mascherbauer J, Bonderman D**. Gender-related differences in heart failure with preserved ejection fraction. *Sci Rep* 8: 1080, 2018.
10. **Fazal L, Laudette M, Paula-Gomes S, Pons S, Conte C, Tortosa F, Sicard P, Sainte-Marie Y, Bisserier M, Lairez O, Lucas A, Roy J, Ghaleb B, Fauconnier J, Mialet-Perez J, Lezoualc'h F**. Multifunctional mitochondrial epac1 controls myocardial cell death. *Circ Res* 120: 645–657, 2017.
11. **Friedberg MK**. Imaging Right-Left Ventricular Interactions. *JACC Cardiovasc Imaging* 11: 755–771, 2018.
12. **Goldstein JA**. Pathophysiology and management of right heart ischemia. *J Am Coll Cardiol* 40: 841–853, 2002.
13. **Gorter TM, Lexis CPH, Hummel YM, Lipsic E, Nijveldt R, Willems TP, van der Horst ICC, van der Harst P, van Melle JP, van Veldhuisen DJ**. Right Ventricular Function After Acute Myocardial Infarction Treated With Primary Percutaneous Coronary Intervention (from the Glycometabolic Intervention as Adjunct to Primary Percutaneous Coronary Intervention in ST-Segment Elevation Myocardial Infarction III Trial). *Am J Cardiol* 118: 338–344, 2016.
14. **Haraldsen P, Lindstedt S, Metzsch C, Algotsson L, Ingemansson R**. A porcine model for acute ischaemic right ventricular dysfunction. *Interact Cardiovasc Thorac Surg* 18: 43–48, 2014.
15. **Harjola V-P, Mebazaa A, Čelutkienė J, Bettex D, Bueno H, Chioncel O, Crespo-Leiro MG, Falk V, Filippatos G, Gibbs S, Leite-Moreira A, Lassus J, Masip J, Mueller C, Mullens W, Naeije R, Nordegraaf AV, Parissis J, Riley JP, Ristic A, Rosano G, Rudiger A, Ruschitzka F, Seferovic P, Sztrymf B, Vieillard-Baron A, Yilmaz MB, Konstantinides S**. Contemporary management of acute right ventricular failure: a statement from the Heart Failure Association and the Working Group on Pulmonary Circulation and Right Ventricular Function of the European Society of Cardiology. *Eur J Heart Fail* 18: 226–241, 2016.
16. **Hein M, Roehl AB, Baumert JH, Scherer K, Steendijk P, Rossaint R**. Anti-ischemic effects of inotropic agents in experimental right ventricular infarction. *Acta Anaesthesiol Scand* 53: 941–948, 2009.
17. **Hoogslag GE, Haeck MLA, Velders MA, Joyce E, Boden H, Schalij MJ, Bax JJ, Ajmone Marsan N, Delgado V**. Determinants of right ventricular remodeling following ST-segment elevation myocardial infarction. *Am J Cardiol* 114: 1490–1496, 2014.
18. **Horan LG, Flowers NC**. Right Ventricular Infarction: Specific Requirements of Management - American Family Physician [Online]. *Am Fam Physician*. https://www.aafp.org/afp/1999/1015/p1727.html.
19. **Jacobs AK, Leopold JA, Bates E, Mendes LA, Sleeper LA, White H, Davidoff R, Boland J, Modur S, Forman R, Hochman JS**. Cardiogenic shock caused by right ventricular infarction: a report from the SHOCK registry. *J Am Coll Cardiol* 41: 1273–1279, 2003.
20. **Kilkenny C, Browne WJ, Cuthill IC, Emerson M, Altman DG**. Improving bioscience research reporting: the ARRIVE guidelines for reporting animal research. *PLoS Biol* 8: e1000412, 2010.

21. **Laster SB, Ohnishi Y, Saffitz JE, Goldstein JA**. Effects of reperfusion on ischemic right ventricular dysfunction. Disparate mechanisms of benefit related to duration of ischemia. *Circulation* 90: 1398–1409, 1994.
22. **Laster SB, Shelton TJ, Barzilai B, Goldstein JA**. Determinants of the recovery of right ventricular performance following experimental chronic right coronary artery occlusion. *Circulation* 88: 696–708, 1993.
23. **Lindsey ML, Bolli R, Canty JM, Du X-J, Frangogiannis NG, Frantz S, Gourdie RG, Holmes JW, Jones SP, Kloner RA, Lefer DJ, Liao R, Murphy E, Ping P, Przyklenk K, Recchia FA, Schwartz Longacre L, Ripplinger CM, Van Eyk JE, Heusch G**. Guidelines for experimental models of myocardial ischemia and infarction. *Am J Physiol Heart Circ Physiol* 314: H812–H838, 2018.
24. **Lindsey ML, Kassiri Z, Virag JAI, de Castro Brás LE, Scherrer-Crosbie M**. Guidelines for measuring cardiac physiology in mice. *Am J Physiol Heart Circ Physiol* 314: H733–H752, 2018.
25. **Lucas A, Mialet-Perez J, Daviaud D, Parini A, Marber MS, Sicard P**. Gadd45γ regulates cardiomyocyte death and post-myocardial infarction left ventricular remodelling. *Cardiovasc Res* 108: 254–267, 2015.
26. **Malinowski M, Proudfoot AG, Eberhart L, Schubert H, Wodarek J, Langholz D, Rausch MK, Timek TA**. Large animal model of acute right ventricular failure with functional tricuspid regurgitation. *Int J Cardiol* 264: 124–129, 2018.
27. **Obradovic S, Dzudovic B, Djuric I, Jovic Z, Djenic N**. Women have right ventricular infarction more frequently than men. *Acta Cardiol* 70: 343–349, 2015.
28. **Ondrus T, Kanovsky J, Novotny T, Andrsova I, Spinar J, Kala P**. Right ventricular myocardial infarction: From pathophysiology to prognosis. *Exp Clin Cardiol* 18: 27–30, 2013.
29. **Popescu BA, Antonini-Canterin F, Temporelli PL, Giannuzzi P, Bosimini E, Gentile F, Maggioni AP, Tavazzi L, Piazza R, Ascione L, Stoian I, Cervesato E, Popescu AC, Nicolosi GL, GISSI-3 Echo Substudy Investigators**. Right ventricular functional recovery after acute myocardial infarction: relation with left ventricular function and interventricular septum motion. GISSI-3 echo substudy. *Heart* 91: 484–488, 2005.
30. **Rallidis LS, Makavos G, Nihoyannopoulos P**. Right ventricular involvement in coronary artery disease: role of echocardiography for diagnosis and prognosis. *J Am Soc Echocardiogr* 27: 223–229, 2014.
31. **Ratliff NB, Peter RH, Ramo BW, Somers WR, Morris JJ**. A model for the production of right ventricular infarction. *Am J Pathol* 58: 471–480, 1970.
32. **Reddy S, Bernstein D**. Molecular Mechanisms of Right Ventricular Failure. *Circulation* 132: 1734–1742, 2015.
33. **Rouhana S, Farah C, Roy J, Finan A, Rodrigues de Araujo G, Bideaux P, Scheuermann V, Saliba Y, Reboul C, Cazorla O, Aimond F, Richard S, Thireau J, Fares N**. Early calcium handling imbalance in pressure overload-induced heart failure with nearly normal left ventricular ejection fraction. *Biochimica et biophysica acta Molecular basis of disease* 1865: 230–242, 2019.
34. **Saleh S, Liakopoulos OJ, Buckberg GD**. The septal motor of biventricular function. *Eur J Cardiothorac Surg* 29 Suppl 1: S126–38, 2006.
35. **Schnelle M, Catibog N, Zhang M, Nabeebaccus AA, Anderson G, Richards DA, Sawyer G, Zhang X, Toischer K, Hasenfuss G, Monaghan MJ, Shah AM**. Echocardiographic evaluation of diastolic function in mouse models of heart disease. *J Mol Cell Cardiol* 114: 20–28, 2018.
36. **Valero-Muñoz M, Backman W, Sam F**. Murine Models of Heart Failure with Preserved Ejection Fraction: a "Fishing Expedition". *JACC Basic to translational science* 2: 770–789, 2017.

Figures Panel

Figure 1: Photographs of various stages of the right coronary ligation surgical method.

Panel A through H, see details in the *Methods* section describing each image. Arrow in F shows RCA. **Panel I:** Representative ECG trace shows ST elevation after RCA ligation. **Panel J:** Kaplan-Meier curve during the peri-surgical period in the sham group (black trace) and in the RCA ligation group (Red trace) (p=0.914; Log-rank Mantel-Cox test). **Panel K:** Kaplan-Meier curve after the peri-surgical period in the sham group (black trace) and in the RCA ligation group (Red trace) (p=0.133, Log-rank Mantel-Cox test).

Figure 2: RCA permanent occlusion induces subsequent RV Cardiac Dysfunction

Panel A: RV global longitudinal strain (n=8/group) variation between Sham (black circle) and RCA ligation (red triangle) mice during 4 weeks follow-up. **Panel B**: RV segmental longitudinal strain (n=8/group) in the mid base free wall and RV apex variation between Sham (black circle) and RCA ligation (red triangle) mice 4 weeks post-MI. **Panel C**: Tricuspid annular plane systolic excursion (TAPSE) measurement between Sham (black circle n=16) and RCA ligation (red triangle n=22) mice during 4 weeks follow-up. **Panel D**: RV/LV area ratio measurement, by echocardiography during diastole, 24h post-surgery (n=16 sham, n=22 RCA ligation) and after 4 weeks between Sham (black circle n=16) and RCA ligation (red triangle n=22). **Panel E**: Representative B-mode four chambers view 4 weeks after RCA ligation. **Panel F:** Diastolic sarcomere length (SL) of cardiomyocytes isolated from RV (n=16-35 cells/group). **Panel G:** Maximal amplitude of SL shortening during contraction of cardiomyocytes. **Panel H:** Contraction velocity. **Panel I:** Relaxation velocity. **Panel J**: Contraction evoked by electrical field stimulation at 0.5 Hz as measured from SL shortening of single intact RV cardiomyocytes 28 days after surgery in Sham (black line) and RCA ligation (red line) ([1]Peak amplitude (µm), $p<0.0001$; [2]Velocity of shortening (µm/sec), $p<0.0001$; [3]Velocity of lengthening (µm/sec), $p<0.0022$) (n=16-35 cells/group). **Panel K:** Representative images and quantification showing cardiac infarct size measured after 24h post RCA ligation. **Panel L:** Representative images of WGA-Cy3 staining in mid-axis section from sham and RCA ligation hearts.

444 A white arrow indicate the location of the ligation. Scale 1mm. **Panel M**: Scar area quantification in
445 the right ventricle in Sham (black circle n=7) and RCA ligation (red triangle n=7) heart. **Panel N**:
446 Interventricular septum thickness measured in Sham (black circle) and RCA ligation (red triangle)
447 hear after 4 weeks.
448 Results are expressed as mean ± SEM. Experimental groups were compared using the Mann-Whitney
449 test for independent samples.
450
451 **Figure 3: Segmental behaviour in the LV : Hypertrophy and hyperkinesia of the septum**
452 **Panel A:** Representative short axis view in Sham group (Top and supplementary video 4) and in RCA
453 ligation group with a D-shaped septum (bottom and supplementary video 5). **Panel B:** Septum
454 thickness measured by B-Mode short axis view during diastole (n=20-26/groups) 28 days after surgery
455 in Sham (black circle) and RCA ligation (red triangle) mice. **Panel C:** Septum circumferential strain
456 (n=21-26/group) 28 days after surgery in Sham (black circle) and RCA ligation (red triangle) mice**.**
457 **Panel D:** Septum circumferential strain rate (n=21-26/group) 28 days after surgery in Sham (black
458 circle) and RCA ligation (red triangle) mice. **Panel E:** Early diastole strain circumferential rate
459 (n=15/groups) 28 days after surgery in Sham (black circle) and RCA ligation (red triangle) mice.
460 **Panel F:** Diastolic sarcomere length (SL) of cardiomyocytes isolated from the septum (n=25-40
461 cells/group). **Panel G:** Maximal amplitude of SL shortening during contraction of cardiomyocytes.
462 **Panel H:** Contraction velocity. **Panel I:** Relaxation velocity.**Panel J**: Contraction evoked by electrical
463 field stimulation at 0.5 Hz as measured from SL shortening of single septal cardiomyocytes 28 days
464 after surgery in Sham (black line) and RCA ligation (red line) ([4]Peak amplitude (µm), $p<0.0004$;
465 [5]Velocity of lengthening (µm/sec), $p<0.017$) (n=25-40 cells/group).
466 Results are expressed as mean ± SEM. Experimental groups were compared using the Mann-Whitney
467 test for independent samples.
468
469
470
471

Figure 4: RCA ligation induced left ventricular diastolic dysfunction

Panel A: Ejection fraction (n=21-26/group) between Sham (black circle) and RCA ligation (red triangle) mice 4 weeks after RV MI. **Panel B:** LV global longitudinal strain (n=16/group) variation between Sham (black circle) and RCA ligation (red triangle) mice 4 weeks after RV MI. **Panel C:** Cardiac output measurement in Sham (black circle) and RCA ligation (red triangle) mice 4 weeks after RV MI (n=16/group). **Panel D:** left ventricle internal dimension during systole (LVIDs) and during diastole (LVIDd) measurement in Sham (black circle) and RCA ligation (red triangle) mice 4 weeks after RV MI (n=21-26/group). **Panel E:** left and right atrium area measurement during diastole in Sham (black circle) and RCA ligation (red triangle) mice 4 weeks after RV MI (n=9-17/group). **Panel F:** Isovolumic relaxation time (IVRT) measurement in Sham (black circle) and RCA ligation (red triangle) mice 4 weeks after RV MI (n=21-25/group). **Panel G:** E/A ratio measurement in Sham (black circle) and RCA ligation (red triangle) mice 4 weeks after RV MI (n=21-25/group). **Panel H:** E/E' ratio measurement in Sham (black circle) and RCA ligation (red triangle) mice 4 weeks after RV MI (n=16/group). **Panel I:** E/SRE ratio measurement in Sham (black circle) and RCA ligation (red triangle) mice 4 weeks after RV MI (n=16-26/group). **Panel J:** Diastolic sarcomere length (SL) of cardiomyocytes isolated from LV (n=22-28 cells/group). **Panel K:** Maximal amplitude of SL shortening during contraction of cardiomyocytes. **Panel L:** Contraction velocity. **Panel M:** Relaxation velocity. **Panel N**: Contraction evoked by electrical field stimulation at 0.5 Hz as measured from SL shortening of single intact LV 28 days after surgery in Sham (black line) and RCA ligation (red line) (^{6}Velocity of shortening (μm/sec), $p<0.001$) (n=22-28 cells/group).

Results are expressed as mean ± SEM. Experimental groups were compared using the Mann-Whitney test for independent samples.

SUPPLEMENTAL DATA

Supplemental video 1: Surgical procedure video of RCA ligation in mice.

Supplemental video 2: Four-chamber view video recorded in B-mode from Sham mice.

500 **Supplemental video 3:** Four-chamber view video recorded in B-mode from RCA ligation mice 4
501 weeks after RV MI.
502 **Supplemental video 4:** Short axis view video recorded in B-mode from Sham mice.
503 **Supplemental video 5:** Short axis view video recorded in B-mode from RCA ligation mice 4 weeks
504 after RV MI.

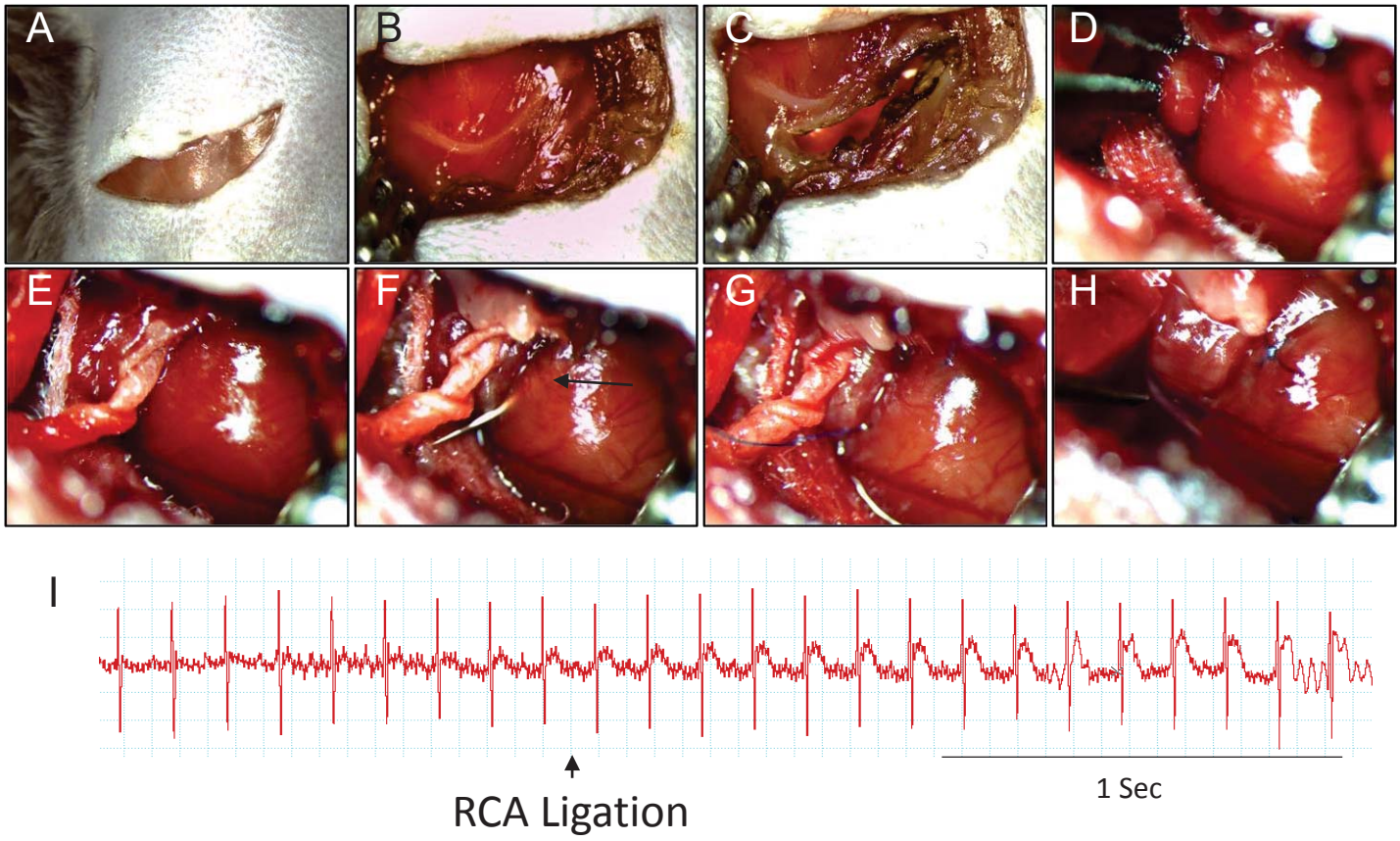
A
B
C
D
E
F
G
H
I
RCA Ligation
1 Sec
J
K
100
80
60
40
Survival (%)
Surgery
p=0.914
0
1
2
3
4
5
6
hour (peri-surgery)
p=0.133
Sham
RCA ligation
0
4
8
12
16
20
24
28
Days (Post-surgery)

Figure 1

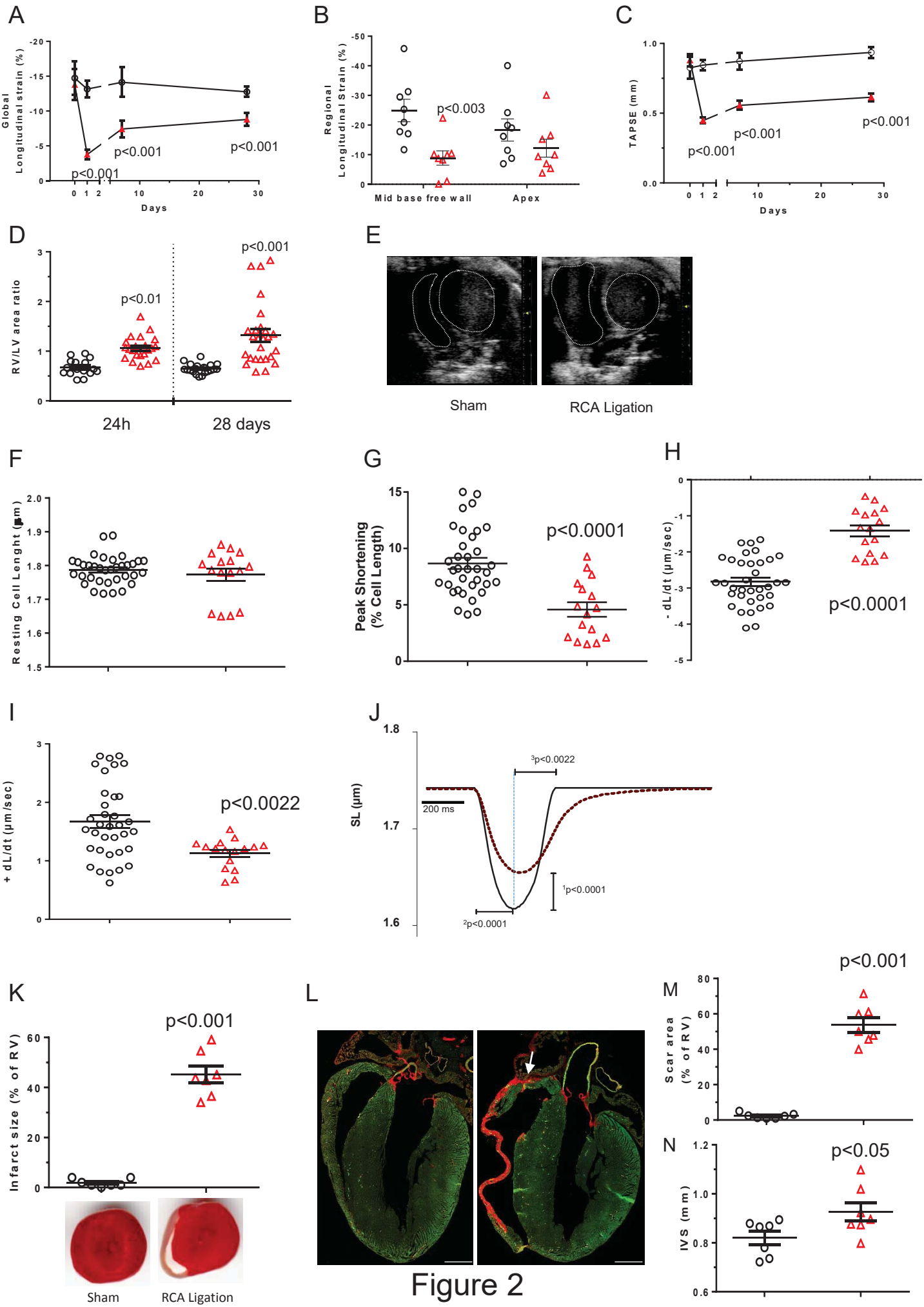
A
Global Longitudinal strain (%)
p<0.001
p<0.001
p<0.001
Days
B
Regional Longitudinal Strain (%)
p<0.003
Mid base free wall
Apex
C
TAPSE (mm)
p<0.001
p<0.001
p<0.001
Days
D
RV/LV area ratio
p<0.01
p<0.001
24h
28 days
E
Sham
RCA Ligation
F
Resting Cell Lenght (µm)
G
Peak Shortening (% Cell Length)
p<0.0001
H
- dL/dt (µm/sec)
p<0.0001
I
+ dL/dt (µm/sec)
p<0.0022
J
SL (µm)
200 ms
3p<0.0022
1p<0.0001
2p<0.0001
K
Infarct size (% of RV)
p<0.001
Sham
RCA Ligation
L
M
Scar area (% of RV)
p<0.001
N
IVS (mm)
p<0.05

Figure 2

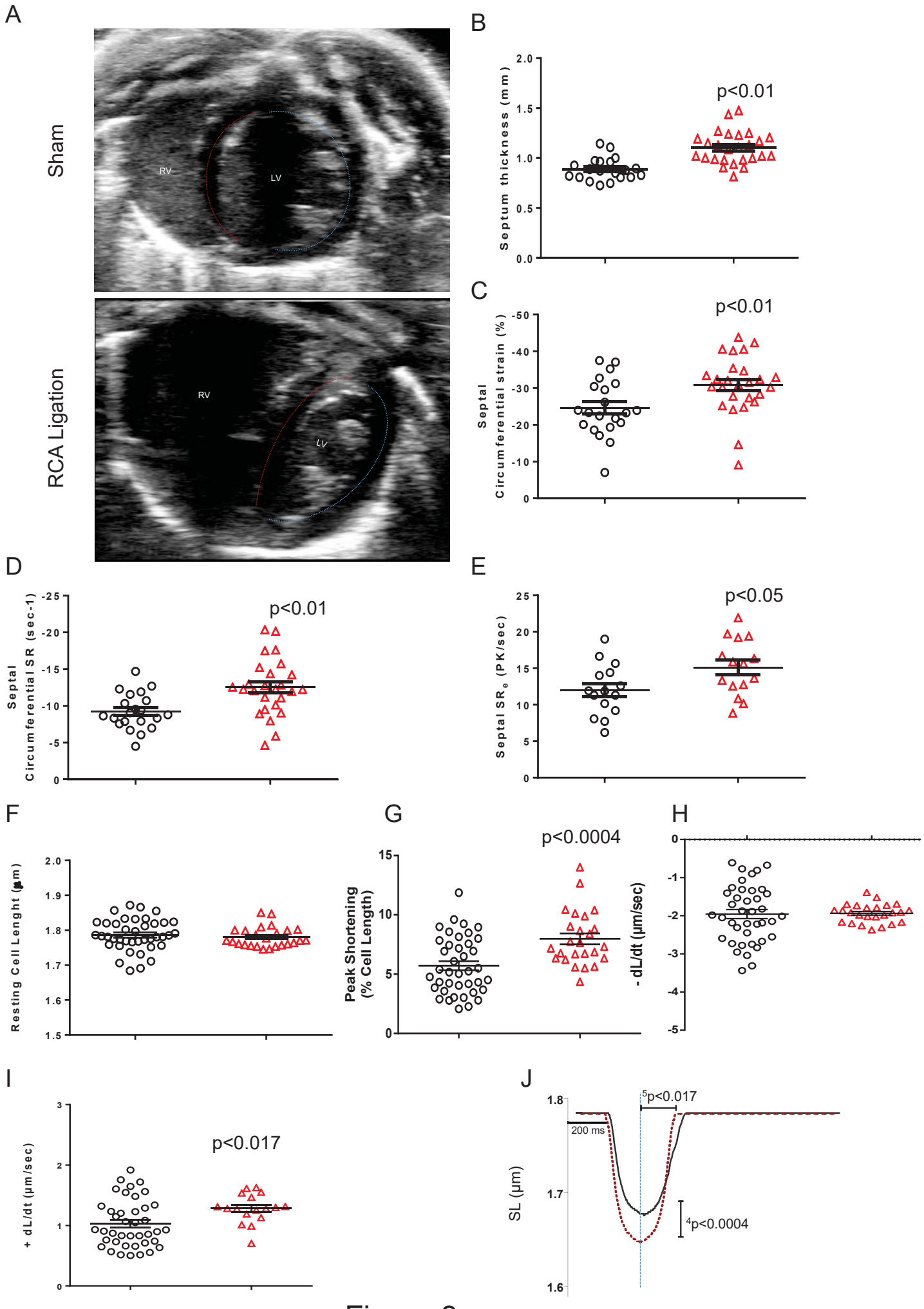
A
Sham
RV
LV
RCA Ligation
RV
LV
B
Septum thickness (mm)
p<0.01
C
Septal Circumferential strain (%)
p<0.01
D
Septal Circumferential SR (sec-1)
p<0.01
E
Septal SRe (PK/sec)
p<0.05
F
Resting Cell Lenght (µm)
G
Peak Shortening (% Cell Length)
p<0.0004
H
- dL/dt (µm/sec)
I
+ dL/dt (µm/sec)
p<0.017
J
SL (µm)
200 ms
5p<0.017
4p<0.0004

Figure 3

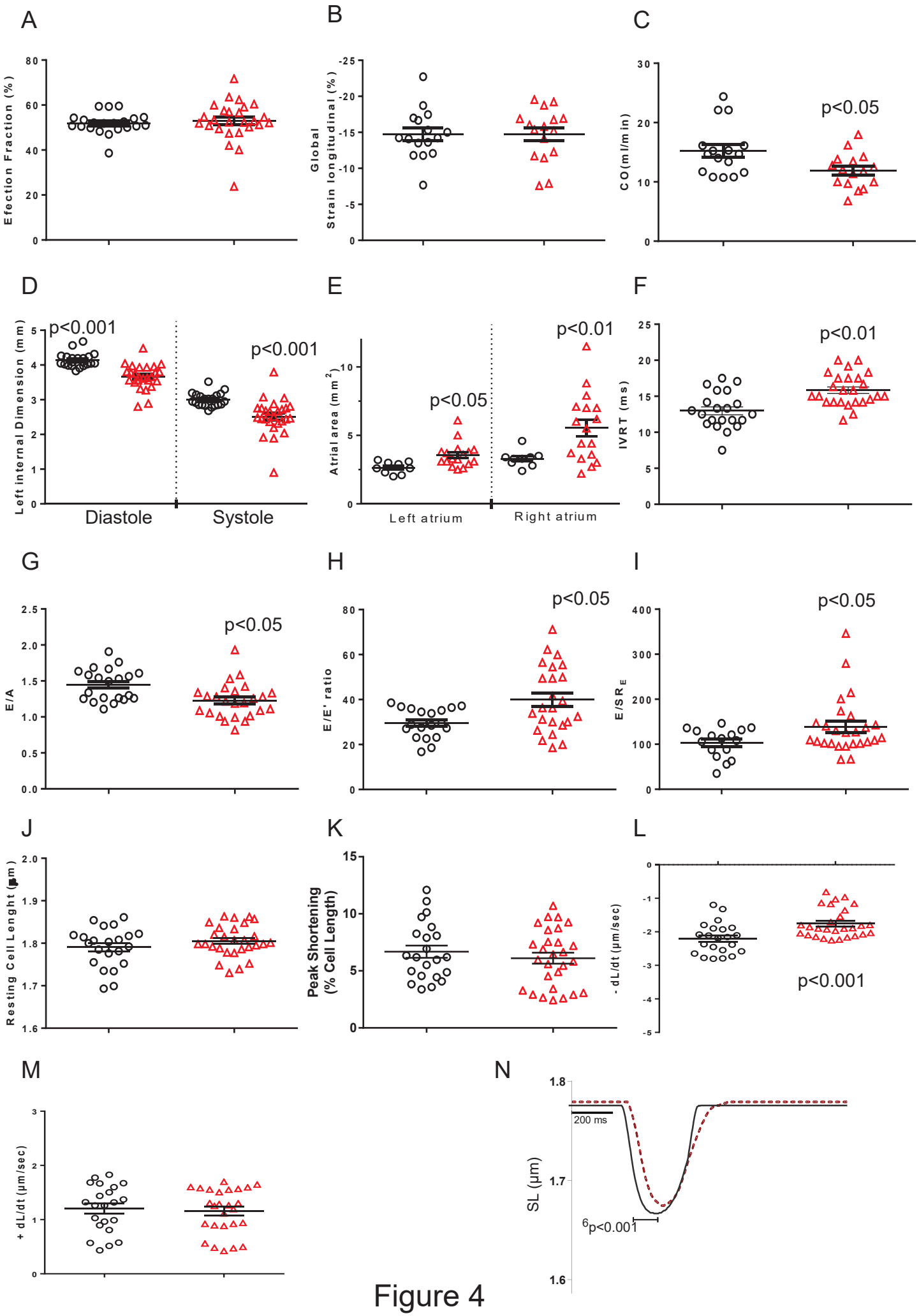
A
Efection Fraction (%)
B
Global Strain longitudinal (%)
C
CO(ml/min)
p<0.05
D
Left internal Dimension (mm)
p<0.001
p<0.001
Diastole
Systole
E
Atrial area (mm²)
p<0.05
p<0.01
Left atrium
Right atrium
F
IVRT (ms)
p<0.01
G
E/A
p<0.05
H
E/E' ratio
p<0.05
I
E/SR_E
p<0.05
J
Resting Cell Lenght (µm)
K
Peak Shortening (% Cell Length)
L
- dL/dt (µm/sec)
p<0.001
M
+ dL/dt (µm/sec)
N
SL (µm)
200 ms
6p<0.001

Figure 4